

A Combination of B- and N-Doped π -Systems Enabling Systematic Tuning of Electronic Structures and Properties

Wenting Sun,^[a] Yue Yang,^[a] Xinyu Tian,^[a] Liuzhong Yuan,^[a] Yue Wang,^[a] and Chuandong Dou^{*[a, b]}

Doping heteroatoms into polycyclic aromatic hydrocarbons (PAHs) may alter their structures and thereby physical properties. This study reports the construction of B/N-codoped PAHs via combining the B- and N-doped π -systems. Two π -extended B/N-codoped PAHs were synthesized through the Mallory photoreaction. Both feature a C₄₈BN₂ π -skeleton, which is assembled by linearly fusing three substructures including B-doped and sp²-hybridized N-doped π -moieties and one pyrene unit. In comparison to the pristine B-doped analog, their intramolecular charge transfer (ICT) states are distinctly modu-

lated by the fused N-doped π -system and the further incorporated cyano group, leading to their tunable optical properties, as revealed by detailed theoretical and experimental analysis. Furthermore, these three molecules have sufficient Lewis acidity and can coordinate with Lewis base to form Lewis acid-base adducts, and notably, such intermolecular complexation can further dynamically modulate their ICT transitions and thereby photophysical properties, such as producing blue, green and red fluorescence.

Introduction

Polycyclic aromatic hydrocarbons (PAHs) have attracted great attention owing to their intriguing optoelectronic, magnetic and spintronic properties and thereby various applications.^[1–5] Doping main-group elements into their π -electron skeletons is an effective strategy to alter the intrinsic structures and physical properties of PAHs by virtue of the characteristic properties of the new heteroatoms.^[6–8] In particular, the B and N atoms owning one less and one more electron than the C atom, respectively, represent two widely employed elements. The incorporation of the B atoms with vacant p orbital into PAHs can afford a variety of B-doped PAH systems (Figure 1a).^[9–15] These molecules were utilized as optoelectronic materials and catalysts, and also may coordinate with Lewis base to form Lewis adducts, which exhibited attractive photo-/thermo-responsive behaviors and control of molecular assembly and diradical characters.^[16–22] The replacement of the CH units in acenes with the sp²-hybridized N atoms can produce azaacenes (N-heteroacenes), which feature higher electron affinity and thus were employed as efficient electron-transporting materials in organic field-effect transistors (Figure 1a).^[23,24] Recently, increasing attention has been paid to simultaneous incorporation of the B and N atoms into PAHs, and remarkably, this

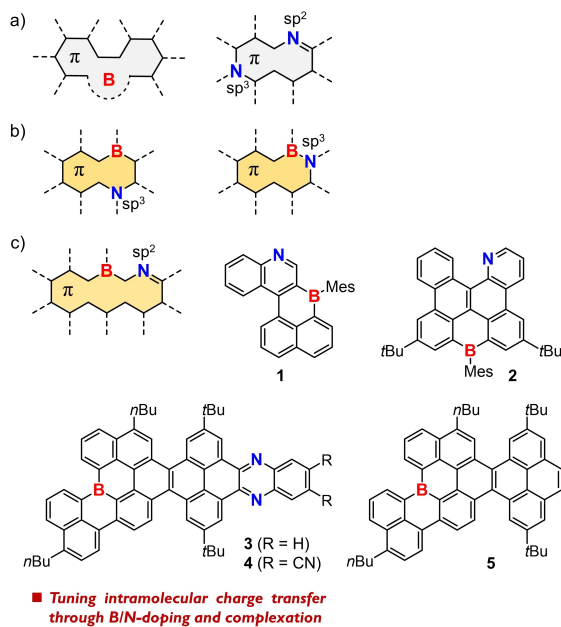


Figure 1. Schematic illustration of PAHs doped with a) B or N atom and b) B and sp³-hybridized N atoms. c) Schematic illustration and the structures of B and sp²-hybridized N atoms codoped PAHs (1–4), along with one B-doped analog (5).

strategy has led to azaborine chemistry and materials (Figure 1b). For example, PAHs doped with well-separated B atoms and sp³-hybridized N atoms exhibit unique multiple resonance effect and highly efficient thermally activated delayed fluorescence (TADF).^[25–29] PAHs doped with the B–N unit represent another important azaborine system, which displays semiconducting and biological properties.^[30–35] Despite of these great advances, PAHs doped with B atom and sp²-hybridized N atom (Figure 1c), have less been explored due to the lack of sufficient synthetic strategy. Until now, only several elegant

[a] W. Sun, Y. Yang, X. Tian, L. Yuan, Prof. Dr. Y. Wang, Prof. Dr. C. Dou
State Key Laboratory of Supramolecular Structure and Materials
College of Chemistry, Jilin University
Changchun 130012 (P. R. China)
E-mail: chuandong@jlu.edu.cn

[b] Prof. Dr. C. Dou
Jiangsu Engineering Laboratory of Novel Functional Polymeric Materials
Soochow University
Suzhou 215123 (P. R. China)

 Supporting information for this article is available on the WWW under
<https://doi.org/10.1002/chem.202302459>

examples have been reported, such as pyridine-embedded PAHs **1** and **2**.^[36,37] Both of the B and sp^2 -hybridized N atoms with electron-withdrawing ability may impact on the electronic characteristics of PAHs, and nevertheless, such effects have not been studied so far.

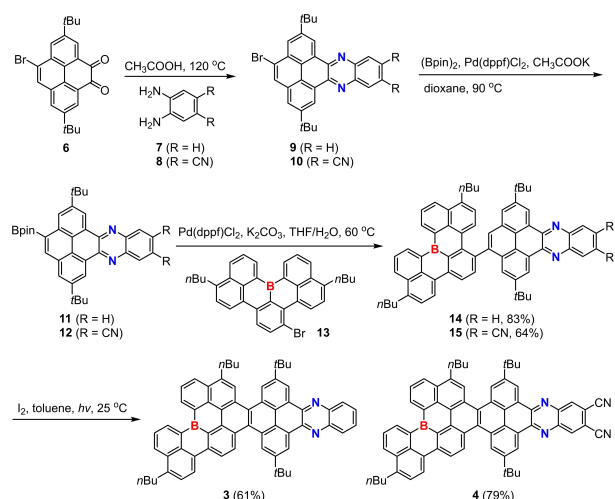
Photochemical reaction is a kind of mild synthetic method to access PAHs and molecular carbon nanostructures. In comparison the classical Scholl cyclization reaction, the Mallory photoreaction can facilitate the formation of multiple C–C bonds and thereby efficient and controllable cyclization.^[38,39] Using this method, a variety of all-carbon and heterocycle-containing PAHs with controlled topologies have been developed, such as contorted or helical molecular nanographenes and nanoribbons.^[40–43] Inspired by Wagner's pioneer work,^[44] we recently disclosed photochemical cyclization on conjugated organoboranes as an effective strategy for rapid π -extension, which affords a new class of B-doped molecular nanoribbons that display semiconducting and photochromism properties.^[45] These studies thus provide a prospective design approach for large-size B/N-codoped PAHs with controlled topologies and tunable properties.

In this study, we report two π -extended B/N-codoped PAHs (**3** and **4**) that were synthesized through the Mallory photoreaction. They feature a $C_{48}BN_2$ π -skeleton composed of three linearly fused substructures including B-doped and sp^2 -hybridized N-doped π -moieties and one pyrene unit. In comparison to the pristine B-doped analog **5**, their intramolecular charge transfer (ICT) states are distinctly modulated by the fused N-doped π -system or the further incorporated cyano group in **4**, leading to their tunable optical properties. In particular, these three molecules can form Lewis acid-base adducts via coordinating with Lewis base, and notably, such intermolecular complexation can further modulate their ICT transitions and thereby photophysical properties, such as producing blue, green and red fluorescence.

Results and Discussion

Our molecular design of these B/N-codoped PAHs is inspired by the efficient synthesis of pyrene-fused azaacenes and B-doped molecular nanoribbons.^[45–48] The diketopyrrolopyrrole moiety can be condensed with aryl diamines to form pyrene-fused azaacenes, which has sufficient reactivity and may be further linearly fused with the B-doped units via photocyclization. A B-doped [4]helicene, first reported by Wagner and Hatakeyama, respectively, was chosen as the key B-doped unit.^[49,50] As shown in Scheme 1, the B-doped [4]helicene, pyrene and quinoxaline are integrated together to obtain two one-dimensional π -extended B/N-codoped PAHs, **3** and **4**.

The target compounds **3** and **4** were synthesized in four steps starting from the diketopyrrolopyrrole precursor **6** (Scheme 1). Condensation of **6** with benzene-1,2-diamine/4,5-diaminophthalonitrile (**7/8**) and then Pd-catalyzed boron esterification of pyrene-fused azaacenes **9/10** afforded the precursors **11/12**. The Suzuki-Miyaura cross-coupling between **11/12** and brominated B-doped [4]helicene **13** produced the key intermediates



Scheme 1. Synthesis of B/N-codoped PAHs **3** and **4**.

14/15. Finally, the Mallory photocyclization reaction using a mercury lamp was performed on **14/15** in the presence of I_2 and air to produce **3/4** in excellent yields via intramolecular cyclization. Compounds **3** and **4** were stable enough to be purified by column chromatography on silica gel. Their chemical structures were confirmed by NMR spectroscopy and high-resolution mass spectrometry (HRMS). As shown in Figure S1, the HRMS spectra show intense signals at $m/z = 862.4432$ for **1** and 912.4313 for **2** along with clear isotopic distributions, which agree well with their calculated molecular mass and simulated patterns (see the Supporting Information), thus corroborating their molecular formulas of $C_{64}H_{55}BN_2$ and $C_{66}H_{53}BN_4$, respectively.

To investigate their molecular configurations, structural optimizations were performed on the model compounds **3'** and **4'** using the density functional theory (DFT) calculations (B3LYP/6-311G(d) level). Both of them feature a $C_{48}BN_2$ π -skeleton that is composed of fourteen hexagonal rings (Figure 2). The B- and N-containing moieties are fused onto one pyrene unit. Notably, the contorted topology is produced owing to the presence of three cove regions, which induced the steric repulsion between the peripheral benzene rings in these regions. The dihedral angles defined by two terminal benzene rings in every cove region are between 29° – 43° .

To reveal the aromaticity of these B/N-codoped PAHs, we conducted nucleus-independent chemical shifts (NICS, B3LYP/6-311+G(d) level) and anisotropy of the induced current densities (ACID, B3LYP/6-311G(d) level) calculations on **3'** and **4'**.^[51] As shown in Figure 2b and 2e, rings A/C/H/I/K of **3'** and **4'** display the largely negative NICS(1)_{ZZ} values, indicating that they are aromatic sextet rings. For rings M/N, the comparably negative NICS(1)_{ZZ} values are observed, suggestive of the well-delocalized electrons in these two aromatic rings. In addition, rings B/F/G in **3'** and **4'** also display very negative NICS(1)_{ZZ} values, proving their aromatic contributions to the π -skeletons. These analyses are in good agreement with the ACID calculations. The ACID plots of **3'** and **4'** show the clockwise diatropic ring currents along the main polycyclic regions and

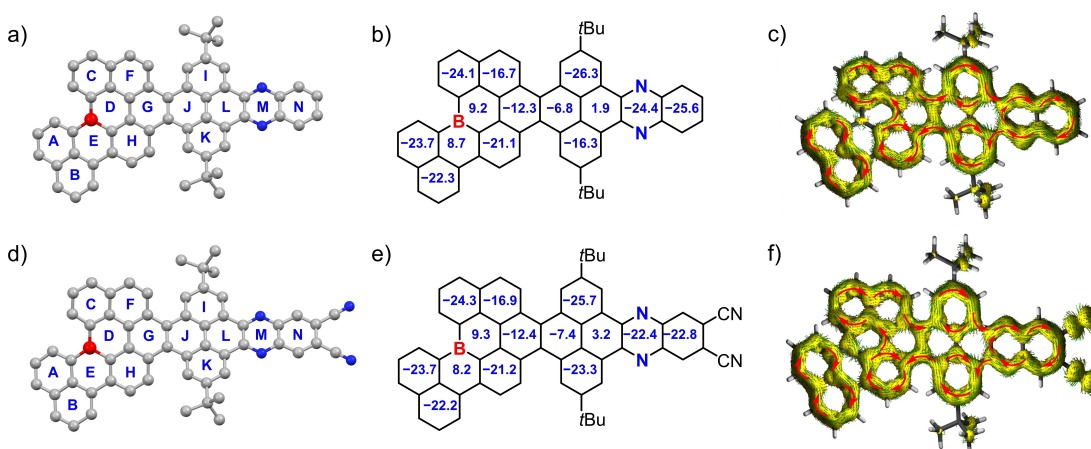


Figure 2. Optimized structures of a) 3' and d) 4'. *n*-Butyl groups and hydrogen atoms are removed for clarity. Calculated NICS(1)_{ZZ} values and ACID plots (contribution from π electrons only) of b,c) 3' and e,f) 4'.

rings A/B, bypass through the benzopyrazine unit and inner paths of pyrene (Figure 2c and 2f). The ACID and NICS results both indicate that such fusion mode contributes to the relatively localized aromatic nature of 3' and 4'.

The photophysical properties of 3 and 4 along with the pristine B-doped analog 5 were investigated. The structure of 5 is shown in Figure 1c and its properties has been reported in the previous work.^[45] Their toluene solutions exhibit two main absorption bands (Figure 3). In the low-energy absorption band, an obvious absorption peak and its shoulder peak (λ_{abs}) are observed at 469/514 nm for 3 and 479/525 nm for 5. For 4, this band is varied to a certain extent, and exhibits the peaks at 467/477/508 nm and a detectable absorption tail that extends to 550 nm. According to the onset absorptions, the optical bandgaps (E_g^{opt}) are determined to be 2.30 eV for 3, 2.18 eV for 4 and 2.26 eV for 5. Their solutions display the yellowish green, yellow and orange fluorescence, respectively. In their fluorescence spectra, they all have one main emission band with the peak at 539 nm for 3, 576 nm for 4 and 551 nm for 5, along with the fluorescence quantum yields of 0.25, 0.28 and 0.16, respectively. In comparison to 5, 3 and 4 display the blue-shifted and red-shifted fluorescence, respectively. Notably, while

the fluorescence spectra of 3 and 5 show a relatively small solvent effect, the emission band of 4 is much more sensitive to the solvent polarity (hexane 549; toluene, 576; THF, 611 nm; acetone, 629 nm), leading to the gradually enlarged Stokes shifts (Figure S3 and Table S2). This solvatochromism behavior along with the absorption tail for 4 is ascribed to its more significant intramolecular charge transfer (CT) state (see below).^[52]

To elucidate the obvious difference in the photophysical properties of 3, 4 and 5, we compared their calculated electronic structures (Figure 4). Density functional theory calculations at the B3LYP/6-311G (d) level show that the LUMOs of 3' and 5' are localized on the B-containing moiety, whereas their HOMOs are well distributed on the pyrene and B-containing moieties except that the HOMO of 3' extends to the N-containing moiety. Thus, in comparison to 5', 3' has a similar LUMO level but a lower HOMO level by 0.16 eV, leading to its

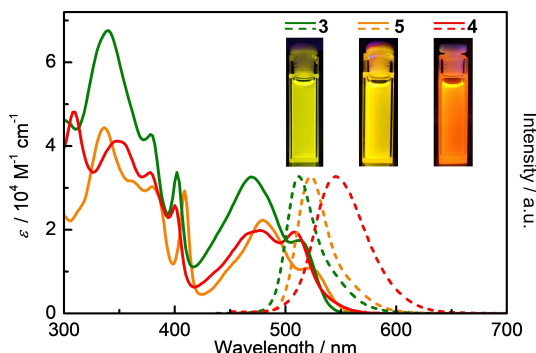


Figure 3. UV/Vis absorption (solid line) and fluorescence (dash line) spectra of 3, 4 and 5 in toluene. Insets are the photographs of the toluene solutions under UV light (365 nm).

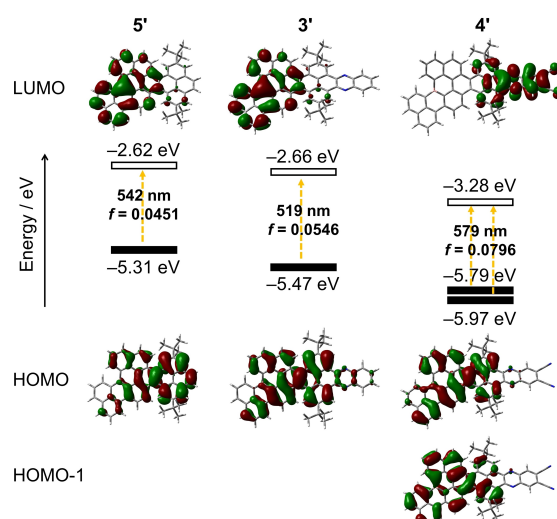


Figure 4. Kohn-Sham molecular orbitals of 3', 4' and 5', together with the wavelengths and oscillator strengths calculated by TD-DFT at the B3LYP/6-311G (d) level of theory.

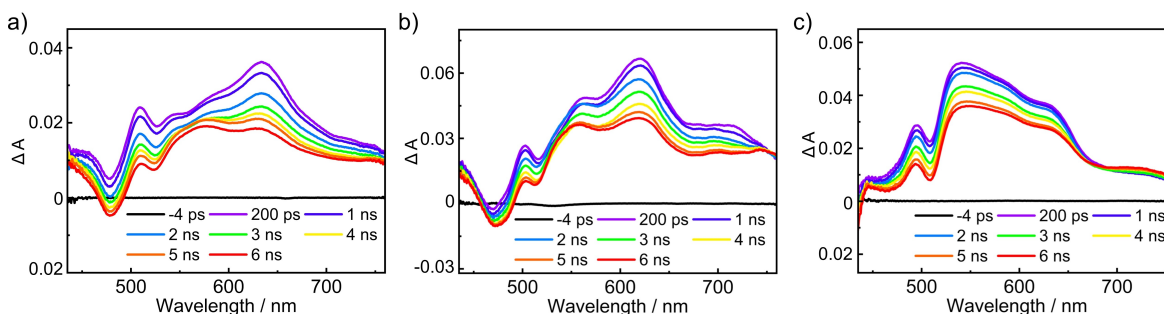


Figure 5. Femtosecond transient absorption spectra of a) 5, b) 3 and c) 4 in toluene.

larger HOMO-LUMO gap (2.81 eV). For **4'**, while the HOMO is also well delocalized on the pyrene and B-containing moieties, the LUMO is significantly changed, namely localization on the N-containing moiety and partial distribution on the pyrene group. These changes are ascribed to the incorporation of the highly electron-deficient cyano groups into **4'**. From **3'** to **4'**, the HOMO and LUMO energy levels are lowered by 0.32 and 0.62 eV, respectively, leading to a smaller HOMO-LUMO gap (2.51 eV) of **4'**. The variation of their calculated HOMO-LUMO gaps agrees well with the changed E_g^{opt} . Time-dependent DFT (TD-DFT) calculations display that the shoulder bands at 514 nm of **3** and 525 nm of **5** are attributed to a forbidden transition involving HOMO→LUMO for **3'** and **5'** (Figure S17). For **4**, the absorption tail is assigned to a forbidden transition involving HOMO→LUMO and HOMO-1→LUMO of **4'**, and the absorption band at 508 nm involves two forbidden $S_0\rightarrow S_2$ and $S_0\rightarrow S_3$ transitions (Figure S18). According to these calculated electronic transitions for low-energy absorption, we can conclude that **4** possesses a much stronger intramolecular CT state that is contributed by the N-containing moiety and the cyano group. Controlled fusion of the B- and N-doped units along with further incorporation of the electron-deficient groups is thus effective to modulate electronic structures of PAHs.

To gain insight into their photophysics, we performed femtosecond transient absorption (fs-TA) spectroscopic measurements on **3**, **4** and **5** in toluene. In the fs-TA spectra (Figure 5), all of them exhibit broad excited-state absorption (ESA) bands. The ground-state bleach (GSB) signals appear at 472/514 nm for **3**, 470/507 nm for **4** and 479/526 nm for **5**, which are in good agreement with their low-energy absorption peaks of the steady-state absorption spectra. Their stimulated emission signals cannot be detected probably because they are completely overwhelmed by their ESA bands. By fitting the decay profiles using single exponential function, the singlet excited-state lifetime (τ) is determined to be 7.2 ns for **3**, 9.3 ns for **4** and 7.1 ns for **5** (Figure S5). The relatively long lifetimes may be ascribed to their radiative relaxation for the singlet excited states and fluorescence behaviors, and there are no complicated internal conversion processes.

The electrochemical properties of **3** and **4** were investigated using cyclic voltammetry with $n\text{Bu}_4\text{NPF}_6$ (0.1 M) as supporting electrolyte. In the cyclic voltammograms (Figure S2), they exhibit two reversible reduction waves with the half-wave

potentials ($E_{1/2}^{\text{red}}$ vs Fc/Fc^+) at $-1.74/-1.94$ eV for **3** and $-1.39/-1.68$ eV for **4** (Table S1). The more positive reduction potential of **4** is ascribed to the strong electron-accepting effect of its cyano groups. Both of **3** and **4** exhibit the irreversible oxidation processes with the first oxidation potentials at $+0.72$ and $+0.81$ eV, respectively, as determined by the differential pulse voltammetry measurements. Accordingly, the electrochemical energy gap (E_g) is calculated to be 2.46 eV for **3** and 2.20 eV for **4**, which are slightly larger and smaller than that (2.42 eV) of **5**, respectively, agreeing well with the variation tendency of their E_g^{opt} .

These B/N-codoped PAHs have Lewis acidity that is induced by the tricoordinate B atoms. We carried out titration experiments on **3** and **4** by monitoring the complexation process using UV/Vis absorption and fluorescence spectroscopies. When adding the Lewis base 4-dimethylaminopyridine (DMAP) into the toluene solution of **3**, the intensity of the absorption bands at 469/514 nm gradually decreased, accompanying appearance of a weak band around 480 nm and two new peaks at 414/363 nm (Figure 6). For **4**, the absorption bands at 477/508 nm gradually disappeared, and a weak band around

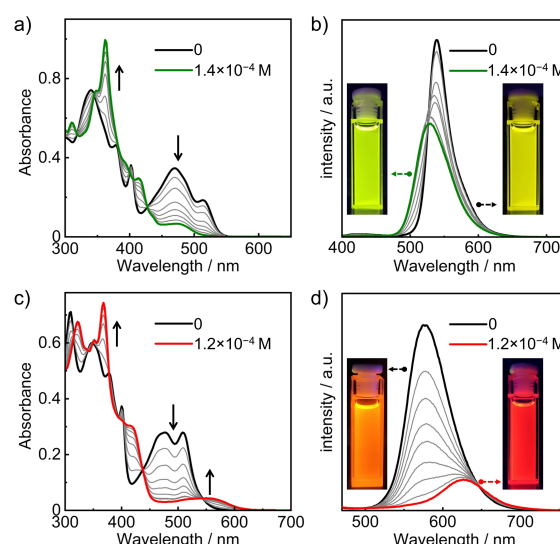


Figure 6. Titrations of a,b) **3** and c,d) **4** in toluene (1×10^{-5} M) with DMAP monitored by UV/Vis absorption and fluorescence spectroscopies. Inset are the photographs of the solutions under UV light (365 nm).

500–600 nm and two new peaks at 416/367 nm were observed. By fitting the titration curves, the constant was determined to be $K = (2.5 \pm 0.07) \times 10^5$ and $(5.1 \pm 0.04) \times 10^5 \text{ M}^{-1}$ for **3** and **4** binding with DMAP, respectively.^[53] In the fluorescence spectra, the addition of DMAP into their solutions leads to the changed fluorescence colors and emission peaks, namely from 539 nm for **3** to 530 nm for **3**-DMAP and from 576 nm for **4** to 627 nm for **4**-DMAP. Therefore, the complexation leads to the simultaneously red-shifted fluorescence and absorption spectra for **4**-DMAP. On the other hand, heating the solution of **3**-DMAP or **4**-DMAP has few effects on the absorption spectra, but greatly impacts on the fluorescence spectra (Figure S7). Higher temperature can recover the emission of **3** or **4** in the presence of excess DMAP. It is thus indicated that the dissociation behavior of **3**-DMAP or **4**-DMAP upon heating and photoexcitation is observed, leading to their dynamic fluorescence properties (Figure S15).^[16,17,45]

We further illustrate the intriguing fluorescence properties of the Lewis adducts doped in polymethyl methacrylate (PMMA), because the molecules can be well dispersed and steadily fixed in these films. As shown in Figure 7, the doped films of **3**-DMAP, **4**-DMAP and **5**-DMAP (doping concentration, 2 wt%) exhibit green, red and blue emissions, respectively. The fluorescence peak is at 528 nm for **3**-DMAP, 609 nm for **4**-DMAP and 450/472 nm for **5**-DMAP, along with the Commission Internationale de l'Éclairage (CIE) coordinates of (0.25, 0.54) for **3**-DMAP, (0.54, 0.45) for **4**-DMAP and (0.14, 0.11) for **5**-DMAP. Therefore, the Lewis coordination leads to the remarkably blue-shifted and red-shifted fluorescence for **5**-DMAP and **4**-DMAP, respectively, comparing with **3**-DMAP. Multiple emitting colors were thus obtained via intermolecular complexation for these three Lewis adducts.

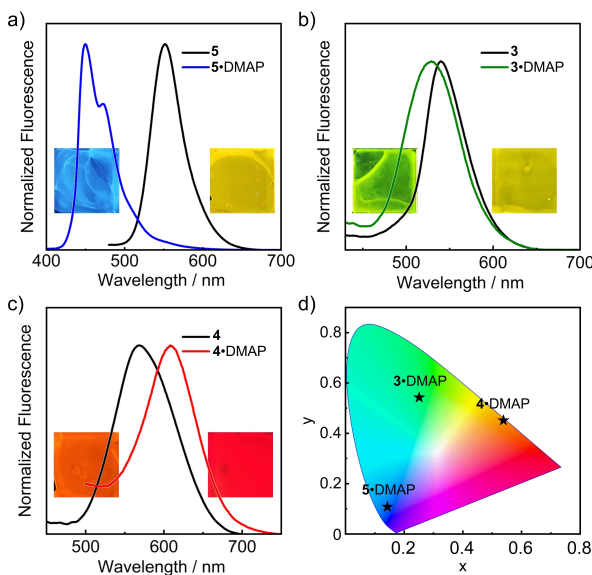


Figure 7. a–c) Fluorescence spectra of the doped films of **3**, **4** and **5**, as well as their Lewis adducts with DMAP. d) CIE color coordinates of the Lewis adducts with DMAP. Inset are the photographs of the doped films under UV light (365 nm).

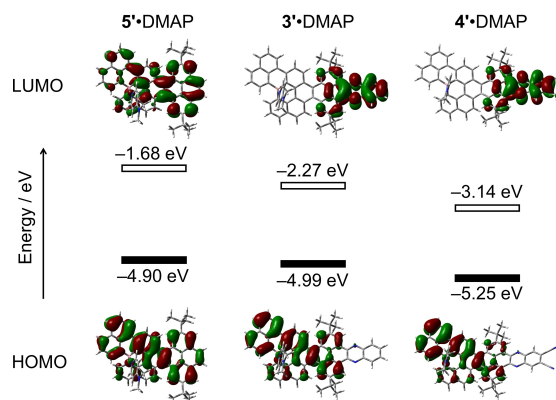


Figure 8. The LUMOs, HOMOs and energy levels of **3**'-DMAP, **4**'-DMAP and **5**'-DMAP calculated at the B3LYP/6-311G (d) level of theory.

Finally, we would like to clarify the electronic effects of Lewis coordination on these three molecules. The Lewis coordination changes the electron distributions and elevate the energies of these complexes to different degrees (Figure 8, Figure S19 and S20). The molecular orbitals of **5**'-DMAP are mostly delocalized over the whole π-skeleton, along with the enlarged bandgap. In contrast, for **3**'-DMAP, while the HOMO is still localized on the B-containing moiety and pyrene group, the LUMO is obviously changed, namely localization on the N-containing moiety and pyrene group, leading to the nearly unchanged bandgap in comparison to **3**. For **4**'-DMAP, the distributions of its HOMO and LUMO are similar with that of **4**', but the bandgap is decreased due to its more enhanced HOMO level. Thus, the electronic effects of Lewis coordination on the B/N-codoped PAHs are closely related to the incorporated N-containing moieties. According to the TD-DFT calculations, **3**'-DMAP exhibits two forbidden $S_0 \rightarrow S_1$ and $S_0 \rightarrow S_2$ transitions that are attributed to the weak absorption band around 480 nm of **3**-DMAP. For **4**'-DMAP, the forbidden $S_0 \rightarrow S_2$, $S_0 \rightarrow S_3$, $S_0 \rightarrow S_4$ and $S_0 \rightarrow S_5$ transitions contribute to the absorption band around 500–600 nm of **4**-DMAP. These calculation results reveal the presence of modulated intramolecular charge transfer states in the complexation process. Therefore, such B/N-codoped PAHs represent a new scaffold for static and dynamic control of intramolecular charge transfer states via fusion and complexation, respectively, and thereby modulation of physical properties of π-system.

Conclusions

We successfully synthesized two π-extended B/N-codoped PAHs through the Mallory photoreaction. Both of them feature a $C_{48}BN_2$ π-skeleton, which is constructed by linearly fusing three substructures including B-doped and sp^2 -hybridized N-doped π-moieties and one pyrene unit. In comparison to the pristine B-doped analog, their intramolecular charge transfer states are distinctly modulated by the fused N-doped π-system and the further incorporated cyano group, leading to their tunable optical properties. Moreover, these three molecules have

sufficient Lewis acidity and can coordinate with Lewis base to form Lewis acid-base adducts, and notably, such intermolecular complexation can further modulate their ICT electronic transitions and thereby optical properties, thus producing blue, green and red fluorescences. This study provides not only a new strategy to design B/N-codoped PAHs but also an alternative approach for systematically modulating physical properties of π -electron systems, which are useful for the development of π -electron materials with desirable functions, such as sensor, photo/thermochromism and laser. Investigations along this line are now in progress in our laboratory.

Supporting Information

The authors have cited additional references within the Supporting Information.^[54–57]

Acknowledgements

This work was financially supported by the Jilin Scientific and Technological Development Program (No. 20220101054JC) and the National Natural Science Foundation of China (No. 22175074).

Conflict of Interests

The authors declare no conflict of interest.

Data Availability Statement

The data that support the findings of this study are available in the Supporting Information of this article.

Keywords: boron • fluorescence • Lewis coordination • nitrogen • polycyclic aromatic hydrocarbons

- [1] A. Narita, X.-Y. Wang, X. Feng, K. Müllen, *Chem. Soc. Rev.* **2015**, *44*, 6616–6643.
- [2] Y. Segawa, H. Ito, K. Itami, *Nat. Rev. Mater.* **2016**, *1*, 15002.
- [3] W. Zeng, J. Wu, *Chem.* **2021**, *7*, 358–386.
- [4] S. H. Pun, Q. Miao, *Acc. Chem. Res.* **2018**, *51*, 1630–1642.
- [5] W. Jiang, Z. Wang, *J. Am. Chem. Soc.* **2022**, *144*, 14976–14991.
- [6] A. Borissov, Y. K. Maurya, L. Moshniahah, W.-S. Wong, M. Źyla-Karwowska, M. Stępień, *Chem. Rev.* **2022**, *122*, 565–788.
- [7] M. Hirai, N. Tanaka, M. Sakai, S. Yamaguchi, *Chem. Rev.* **2019**, *119*, 8291–8331.
- [8] J. Feng, Y. Wu, Q. Yu, Y. Liu, W. Jiang, D. Wang, Z. Wang, *CCS Chem.* **2022**, *2*, 271–279.
- [9] L. Ji, S. Griesbeck, T. B. Marder, *Chem. Sci.* **2017**, *8*, 846–863.
- [10] E. v. Grotthuss, A. John, T. Kaese, M. Wagner, *Asian J. Org. Chem.* **2018**, *7*, 37–53.
- [11] A. Escande, M. J. Ingleson, *Chem. Commun.* **2015**, *51*, 6257–6274.
- [12] J. M. Farrell, C. Mützel, D. Bialas, M. Rudolf, K. Menekse, A.-M. Krause, M. Stolte, F. Würthner, *J. Am. Chem. Soc.* **2019**, *141*, 9096–9104.
- [13] L. Yuan, J. Guo, Y. Yang, K. Ye, C. Dou, Y. Wang, *CCS Chem.* **2023**, *5*, 876–884.
- [14] F. Vidal, F. Jäkle, *Angew. Chem. Int. Ed.* **2019**, *58*, 5846–5870.
- [15] Z. Huang, S. Wang, R. D. Dewhurst, N. V. Ignat'ev, M. Finze, H. Braunschweig, *Angew. Chem. Int. Ed.* **2020**, *59*, 8800–8816.
- [16] N. Ando, T. Yamada, H. Narita, N. N. Oehlmann, M. Wagner, S. Yamaguchi, *J. Am. Chem. Soc.* **2021**, *143*, 9944–9951.
- [17] K. Matsuo, S. Saito, S. Yamaguchi, *J. Am. Chem. Soc.* **2014**, *136*, 12580–12583.
- [18] J. Guo, Y. Yang, C. Dou, Y. Wang, *J. Am. Chem. Soc.* **2021**, *143*, 18272–18279.
- [19] H. Narita, H. Choi, M. Ito, N. Ando, S. Ogi, S. Yamaguchi, *Chem. Sci.* **2022**, *13*, 1484–1491.
- [20] R. J. Kahan, D. L. Crossley, J. Cid, J. E. Radcliffe, M. J. Ingleson, *Angew. Chem. Int. Ed.* **2018**, *57*, 8084–8088.
- [21] J. Guo, Z. Li, X. Tian, T. Zhang, Y. Wang, C. Dou, *Angew. Chem. Int. Ed.* **2023**, *62*, e202217470.
- [22] Z. Fan, W. Sun, Y. Yang, J. Guo, C. Dou, Y. Wang, *Chin. Chem. Lett.* **2023**, *34*, 107729.
- [23] U. H. Bunz, *Acc. Chem. Res.* **2015**, *48*, 1676–1686.
- [24] Q. Miao, *Adv. Mater.* **2014**, *26*, 5541–5549.
- [25] T. Hatakeyama, K. Shiren, K. Nakajima, S. Nomura, S. Nakatsuka, K. Kinoshita, J. Ni, Y. Ono, T. Ikuta, *Adv. Mater.* **2016**, *28*, 2777–2781.
- [26] M. Yang, I. S. Park, T. Yasuda, *J. Am. Chem. Soc.* **2020**, *142*, 19468–19472.
- [27] Y. Zhang, D. Zhang, J. Wei, Z. Liu, Y. Lu, L. Duan, *Angew. Chem. Int. Ed.* **2019**, *58*, 16912–16917.
- [28] W. Yang, N. Li, J. Miao, L. Zhan, S. Gong, Z. Huang, C. Yang, *CCS Chem.* **2022**, *4*, 3463–3471.
- [29] Y. Xu, C. Li, Z. Li, J. Wang, J. Xue, Q. Wang, X. Cai, Y. Wang, *CCS Chem.* **2022**, *4*, 2065–2079.
- [30] K. Zhao, Z.-F. Yao, Z.-Y. Wang, J.-C. Zeng, L. Ding, M. Xiong, J.-Y. Wang, J. Pei, *J. Am. Chem. Soc.* **2022**, *144*, 3091–3098.
- [31] C. R. McConnell, S.-Y. Liu, *Chem. Soc. Rev.* **2019**, *48*, 3436–3453.
- [32] J. Ruhl, N. Oberhof, A. Dreuw, H. A. Wegner, *Angew. Chem. Int. Ed.* **2023**, *62*, e202300785.
- [33] W. Zhang, G. Li, L. Xu, Y. Zhuo, W. Wan, N. Yan, G. He, *Chem. Sci.* **2018**, *9*, 4444–4450.
- [34] T. Kaehler, M. Bolte, H.-W. Lerner, M. Wagner, *Angew. Chem. Int. Ed.* **2019**, *58*, 11379–11384.
- [35] J.-Y. Wang, J. Pei, *Chin. Chem. Lett.* **2016**, *27*, 1139–1146.
- [36] D. L. Crossley, R. J. Kahan, S. Endres, A. J. Warner, R. A. Smith, J. Cid, J. J. Dunsford, J. E. Jones, I. Vitorica-Yrezabal, M. J. Ingleson, *Chem. Sci.* **2017**, *8*, 7969–7977.
- [37] V. M. Hertz, J. G. Massoth, M. Bolte, H.-W. Lerner, M. Wagner, *Chem. Eur. J.* **2016**, *22*, 13181–13188.
- [38] M. Stepień, E. Gońska, M. Źyla, N. Sprutta, *Chem. Rev.* **2017**, *117*, 3479–3716.
- [39] D. M. Baier, C. Spula, S. Fanenstich, S. Grätz, L. Borchardt, *Angew. Chem. Int. Ed.* **2023**, *62*, e202218719.
- [40] N. Liang, D. Meng, Z. Wang, *Acc. Chem. Res.* **2021**, *54*, 961–975.
- [41] B. Liu, M. Böckmann, W. Jiang, N. L. Doltsinis, Z. Wang, *J. Am. Chem. Soc.* **2020**, *142*, 7092–7099.
- [42] V. M. Hertz, H.-W. Lerner, M. Wagner, *Org. Lett.* **2015**, *17*, 5240–5243.
- [43] T. J. Sisto, Y. Zhong, B. Zhang, M. T. Trinh, K. Miyata, X. Zhong, X.-Y. Zhu, M. L. Steigerwald, F. Ng, C. Nuckolls, *J. Am. Chem. Soc.* **2017**, *139*, 5648–5651.
- [44] V. M. Hertz, M. Bolte, H.-W. Lerner, M. Wagner, *Angew. Chem. Int. Ed.* **2015**, *54*, 8800–8804.
- [45] W. Sun, J. Guo, Z. Fan, L. Yuan, K. Ye, C. Dou, Y. Wang, *Angew. Chem. Int. Ed.* **2022**, *61*, e202209271.
- [46] Z. Wang, P. Gu, G. Liu, H. Yao, Y. Wu, Y. Li, G. Rakesh, J. Zhu, H. Fu, Q. Zhang, *Chem. Commun.* **2017**, *53*, 7772–7775.
- [47] F. Hernández-Culebras, M. Melle-Franco, A. Mateo-Alonso, *Angew. Chem. Int. Ed.* **2022**, *61*, e202205018.
- [48] A. H. Endres, M. Schaffroth, F. Paulus, H. Reiss, H. Wadeppohl, F. Rominger, R. Krämer, U. H. F. Bunz, *J. Am. Chem. Soc.* **2016**, *138*, 1792–1795.
- [49] K. Schickedanz, T. Trageser, M. Bolte, H.-W. Lerner, M. Wagner, *Chem. Commun.* **2015**, *51*, 15808–15810.
- [50] F. Miyamoto, S. Nakatsuka, K. Yamada, K.-i. Nakayama, T. Hatakeyama, *Org. Lett.* **2015**, *17*, 6158–6161.
- [51] M. Randić, *Chem. Rev.* **2003**, *103*, 3449–3605.
- [52] C. Dou, S. Saito, S. Yamaguchi, *J. Am. Chem. Soc.* **2013**, *135*, 9346–9349.
- [53] F. Jäkle, *Chem. Rev.* **2010**, *110*, 3985–4022.
- [54] L. Ji, I. Krummenacher, A. Friedrich, A. Lorbach, M. Haehnel, K. Edkins, H. Braunschweig, T. B. Marder, *J. Org. Chem.* **2018**, *83*, 3599–3606.

- [55] X. Li, S. Zhang, W. Chen, H. Han, M. Qiu, J. Chen, Q. Zhang, *Chem. Eur. J.* **2022**, *28*, e202103808.
- [56] P. Thordarson, *Chem. Soc. Rev.* **2011**, *40*, 1305–1323.
- [57] Gaussian 09, Revision A.02, M. J. Frisch, G. W. Trucks, H. B. Schlegel, G. E. Scuseria, M. A. Robb, J. R. Cheeseman, G. Scalmani, V. Barone, G. A. Petersson, H. Nakatsuji, X. Li, M. Caricato, A. V. Marenich, J. Bloino, B. G. Janesko, R. Gomperts, B. Mennucci, H. P. Hratchian, J. V. Ortiz, A. F. Izmaylov, J. L. Sonnenberg, D. Williams-Young, F. Ding, F. Lipparini, F. Egidi, J. Goings, B. Peng, A. Petrone, T. Henderson, D. Ranasinghe, V. G. Zakrzewski, J. Gao, N. Rega, G. Zheng, W. Liang, M. Hada, M. Ehara, K. Toyota, R. Fukuda, J. Hasegawa, M. Ishida, T. Nakajima, Y. Honda, O. Kitao, H. Nakai, T. Vreven, K. Throssell, J. A. Montgomery, Jr., J. E. Peralta, F. Ogliaro, M. J. Bearpark, J. J. Heyd, E. N. Brothers, K. N. Kudin, V. N. Staroverov, T. A. Keith, R. Kobayashi, J. Normand, K. Ragahavachari, A. P. Rendell, J. C. Burant, S. S. Iyengar, J. Tomasi, M. Cossi, J. M. Millam, M. Klene, C. Adamo, R. Cammi, J. W. Ochterski, R. L. Martin, K. Morokuma, O. Farkas, J. B. Foresman, D. J. Fox, Gaussian, Inc., Wallingford CT, 2009.

Manuscript received: July 30, 2023

Accepted manuscript online: August 28, 2023

Version of record online: October 9, 2023
